Modification of the spontaneous emission rate of Eu^{3+} ions embedded within a dielectric layer above a silver mirror

P. T. Worthing, R. M. Amos,* and W. L. Barnes
Thin Film Photonics Group, Department of Physics, University of Exeter, Stocker Road, Exeter, Devon EX4 4QL, United Kingdom
(Received 27 March 1998)

We investigate the spontaneous emission rate of Eu^{3+} ions in an asymmetric microcavity. The cavity consists of a thin dielectric layer bounded on one side by silver and on the other by air. Samples were constructed using the Langmuir-Blodgett technique, the emitters being incorporated as a single monolayer within the microcavity. This technique allowed both the cavity thickness and the position of the emitters within it to be controlled to one monolayer ($\approx$2.6 nm). Measurements are presented of the spontaneous emission decay rate as a function of both the dielectric layer thickness and the position of the emitters within the layer. We find good agreement between our data and a classical model. The model allows us to investigate the role of the electromagnetic modes of the microcavity in controlling the spontaneous emission decay rate of the emitters. In particular, we are able to evaluate the contribution each of the modes makes to the decay. We discuss the implication these results may have in increasing the photoluminescence efficiency from microcavity based emissive devices. [S1050-2947(99)03501-5]

PACS number(s): 42.50.−p, 42.55.Sa, 73.20.Mf, 42.79.Gn

I. INTRODUCTION

It is now commonly accepted that spontaneous emission (SpE) is not an immutable property of the emitter, rather, it depends on the photonic mode density (PMD) at the location of the emitter. This was originally noted by Purcell [1] and is embodied in Fermi's golden rule [2]. The photonic mode density is easily modified by changing the electromagnetic (EM) boundary conditions and perhaps the simplest system showing significant changes to the PMD is the single planar mirror. Drexhage [3] examined the spontaneous emission rate of Eu^{3+} ions as a function of their separation from a metallic mirror. This was the first experimental demonstration that the SpE rate was dependent on PMD in the optical regime. Drexhage found that the lifetime of the Eu^{3+} ions showed a damped oscillatory dependence on the emitter mirror separation (d_{bot}) for separations greater than 100 nm, see Fig. 1, while quenching associated with nonradiative transfer to the metal dominated for $d_{\mathrm{bot}} < 100$ nm.

The sample geometry used by Drexhage comprised a monolayer containing Eu^{3+} ions separated from the metallic mirror by transparent organic monolayers. This geometry is shown in the inset of Fig. 1; notice that in addition to the metallic mirror a second reflective interface is present, between the dielectric and the semi-infinite air half space above. A model that considers the emitters to be forced, damped electric dipole oscillators was developed by Chance, Prock, and Silbey (CPS) [4] and was used to model the data of Drexhage. The model considers the dipole forcing term to arise from the reflection of the dipole field brought about by the presence of an interface. The oscillation in the SpE lifetime as a function of the emitter-metal separation (d_{bot}) is therefore due to the retardation of the reflected field, caused by the emitter-mirror separation. It has been noted that to achieve the best agreement between the experimental results and the CPS model the second interface (dielectric-air) must be incorporated within the model [4]. The need to include the effect of this interface may appear somewhat surprising given its low reflectivity, especially when compared to that of the metallic-dielectric interface.

The focus of several previous studies has been to investigate the role of the mirror. Drexhage and others [5] have reported lifetime measurements above metals, while other investigators have studied semiconductor mirrors [6]. However, as noted above, the second interface also plays an important role. In particular, the presence of the second interface may lead to the structure supporting waveguide modes. Waveguide modes associated with symmetrical cavities formed from two highly reflecting mirrors (e.g., two metal mirrors) have been extensively investigated [7]. As the thickness of these cavities is increased new waveguide modes may be supported by the cavity. The introduction of these

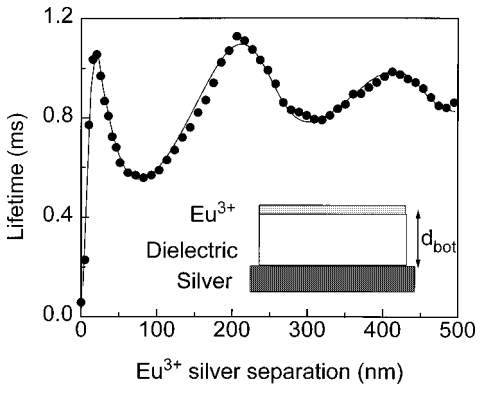

FIG. 1. Spontaneous emission lifetime of Eu^{3+} ions located in the top monolayer of a thin dielectric layer above an opaque silver mirror, as a function of the Eu^{3+}-mirror separation d_{bot}. The dots are the experimental data, the theory, described in the text, is shown as a solid line. The inset shows a schematic of the sample structure.

*Present address: DERA (Malvern), St. Andrews Road, Malvern, Worcs WR14 3PS, U.K.

modes has been observed to cause significant, sharp changes in the SpE rate of emitters located in these high Q cavities as the cavity thickness was changed [8]. The role of such modes in dictating the SpE rate has been thoroughly investigated [9]. However, less attention has been paid to the role of the waveguide modes in the asymmetric type of cavity shown in the inset of Fig. 1. Most previous experimental work in this area has concentrated on looking at changes in the intensity of the emission [10], typically normal to the microcavity. Here we focus our attention on the SpE rate of the emitters because such measurements, in conjunction with a theoretical model, allow us to quantify the contribution of the various modes of the structure to the SpE rate.

The asymmetric microcavity studied here shows a different behavior when compared to that of the more familiar symmetric microcavity. This difference arises because the reflectivity of a dielectric-air interface has a strong angular dependence; ranging from weakly reflecting at normal incidence to perfectly reflecting at angles greater than the critical angle associated with total internal reflection. It is the investigation of the role of the EM modes of the asymmetric microcavity in determining the SpE rate of emitters located within it that forms the subject of the work reported here.

II. OUTLINE OF THE INVESTIGATION

We used the Langmuir-Blodgett technique to embed a monolayer containing Eu^{3+} ions within a thin dielectric layer above a planar metal mirror. This technique allowed us to achieve nanometer precision of both the emitter-mirror separation (d_{bot}) and the emitter-air separation (d_{top}). We have measured the SpE lifetime of the emitters embedded at various positions within the dielectric film for a variety of film thicknesses. As we shall see, the comparison of our data with a theoretical model allows us to examine the role of the different modes of these asymmetric microcavities in controlling spontaneous emission. Our investigation comprises three parts.

(1) Initially we investigated the effect on the SpE lifetime of the air-emitter separation d_{top} for different values of d_{bot} thus showing the importance of the top interface.

(2) Second, we investigated how placing the emitter at different positions within a fixed thickness film modifies the SpE rate. This highlights the importance of the position of the emitters in determining the coupling to the different EM modes of the structure.

(3) Finally, we varied the total dielectric thickness while maintaining the emitters at a fixed distance from the silver mirror. By choosing appropriate cavity thicknesses we were able to span the transition of the first TE waveguide mode from being radiative in nature to that of a well-guided one, see Fig. 2(a). We shall see that although there is no significant modification to the SpE rate when this transition occurs, modeling shows that there is a change in the contributions the different decay channels make to the decay of the emitter.

The nature of the modes associated with the symmetric and asymmetric microcavities, and in particular the differences between them, are readily discussed by looking at the dispersion of the modes in the two structures. In the next section we outline a theoretical model that allows us to calculate the dispersion of the modes, and which, in addition, allows us to evaluate the contribution each mode makes to the SpE decay rate.

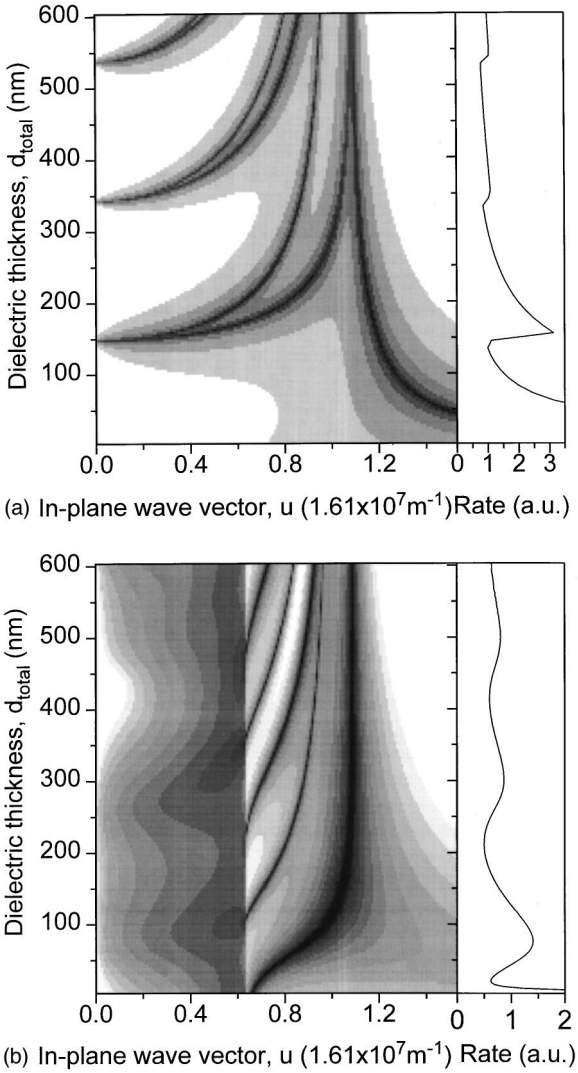

FIG. 2. (a) shows a gray scale map of $I(u)$ for a symmetric metal clad microcavity as a function of the in-plane wave vector u and the dielectric thickness d_{total}. (b) is for the metal-dielectric-air asymmetric microcavity. The dipoles are chosen to be located such that $d_{\mathrm{bot}}=0.4\times d_{\mathrm{total}}$. The gray scale is chosen such that the dark regions represent large contributions to the SpE decay rate and the scale used is logarithmic. The plot on the right-hand side shows the integration of $I(u)$ over all values of u for each value of the dielectric thickness; it thus shows the decay rate as a function of the total dielectric thickness. For (a) this plot is characteristic of the decay rate for an emitter in a high Q metallic microcavity.

III. THEORETICAL MODEL

The theory developed by CPS [4] is well established for modeling the modification to the spontaneous emission rate of an emitter due to the presence of infinite planar interfaces. The theory considers the emitter to be an oscillating electric dipole, which is damped owing to the fact that it radiates. The presence of the interface is incorporated by allowing the reflected dipole field to act as a driving field; the dipole is thus forced. The modification in the decay rate for an isotro-

pic distribution of dipole orientations (b_{iso}) can then be written as

$$\frac{b_{\mathrm{iso}}}{b_0} = (1-q) + q\,\frac{1}{2}\,\mathrm{Im}\int_0^\infty I(u)\,du, \tag{1}$$

where q is quantum efficiency of the dipole and b_0 is radiative decay rate, in the absence of any interfaces. The function $I(u)$ is a measure of the power lost as a function of the in-plane wave vector [4]. It depends upon the location and the Fresnel reflection coefficients of the planar interfaces in the microcavity. The parameter u is the component of the wave vector in the plane of the interfaces, normalized with respect to the wave vector of the radiation in the far field. It is well known that a dipole near a surface can couple to modes having wave vectors greater than that available to the far field of the dipole [11]. This is due to higher wave vector components being present in the near field of the dipole; therefore the integration in Eq. (1) must be performed over all positive values of u.

A number of parameters are required for this model; these include the dielectric constants of the silver, the air, and the dielectric cavity material (these allow the Fresnel reflection coefficients to be evaluated). The dielectric constant of silver was taken to be $\varepsilon = -16.0 + 0.6i$, consistent with other measurements of evaporated films [12]. In the model it is assumed that the monolayers used as the transparent spacer layers are optically isotropic. This is known to be an approximation [13], although previous work has shown that the use of an average isotropic value for the permittivity ($\varepsilon = 2.49 + 0.0i$) gives an excellent approximation for the type of work considered here [14]. The thickness of each monolayer was taken to be approximately 2.6 nm [4] and a small variation ($\sim$2%) was allowed in fitting the theory to the data to account for variations in deposition conditions. The emissive monolayer was assumed to have the same dielectric constant and thickness as one transparent spacer monolayer, with the dipole emitter centrally located within it.

The function $I(u)$ is a measure of the contribution to the SpE rate of the emitter as a function of the normalized in-plane component of the wave vector, u. The normalized in-plane wave vector associated with the condition for total internal reflection for our dielectric-air interface is $u = 0.634$. Thus modes with values of $0 < u < 0.634$ have propagating far-field components in the semi-infinite air half space; we shall refer to these as radiative. Modes with values of $u > 0.634$ have evanescent field components in the semi-infinite air half space, and are therefore bound to the cavity medium.

It should be noted that the dispersion of the EM modes of the system is only dependent on the optical structure of the microcavity. Since we assume that the dipole emitter has the same dielectric constant as the transparent spacer layers the location of the emitter has no influence on the dispersion of the modes. The location of the emitter does, however, strongly affect the coupling between the emitter and the various modes [15]. To compare the dispersion of the modes in the symmetric (metal-dielectric-metal) and asymmetric (metal-dielectric-air) microcavity we can investigate $I(u)$ as a function of the cavity thickness (d_{total}). Figures 2(a) and 2(b) display $I(u)$, in the form of a gray scale map, as a function of u and the thickness of the dielectric layer for the symmetric and asymmetric microcavity. Here the position of the emitters is chosen such that $d_{\mathrm{bot}} = \frac{2}{5} d_{\mathrm{total}}$, in the dielectric layer. Black regions represent a large contribution to the SpE rate, thus indicating the presence of a decay channel.

For the metal-dielectric-metal symmetric cavity, Fig. 2(a), the modes can be classified by their asymptotic value at large cavity thickness. The two modes that converge at a value of $u = 1.08$ are the coupled surface plasmon polaritons (SPP) of the metal clad cavity [16]. The asymptotic value of u for large d_{total} for these SPP modes agrees well with the values expected for a single dielectric metal interface [17]. The modes which have an asymptotic value $u = 1$ correspond to the waveguide modes of the microcavity. Note that each waveguide mode has a clearly defined cutoff thickness, below which it does not exist. Above the cutoff thickness the dispersion of the mode has a smooth continuous nature with increasing thickness. If we now compare this to the asymmetric case (metal-dielectric-air), Fig. 2(b), the presence of a single metal-dielectric interface dictates that there is only one SPP mode, again asymptotic at large d_{total} with $u = 1.08$. Also seen are the waveguide modes; they have an asymptotic value of $u = 1.0$ at large d_{total}, but in contrast to the symmetrical case these modes are not well defined for all values of u less than 1. For values of $u < 0.634$, total internal reflection no longer occurs at the dielectric-air interface and the modes are no longer confined to the cavity. In this regime, the modes are frequently referred to as leaky in order to describe their radiative nature.

The insets, to the right of Figs. 2(a) and 2(b), show the result of integrating $I(u)$, over all positive values of u, for the different values of d_{total} and thus show the modification of the SpE rate, see Eq. (1). We note that for the metal-dielectric-metal clad system the introduction of a new waveguide mode is accompanied by a sharp feature in the SpE rate. For the metal-dielectric-air SpE rate there are no such sharp features.

We have seen above that the emitters embedded within microcavities may lose their energy through three different decay channels; radiative (leaky) modes, waveguide modes, and the SPP modes. We now examine the relative importance of these decay channels as a function of the emitter location within various structures by comparing the results of experimental measurements with the theory outlined above.

IV. EXPERIMENT

The experimental technique used here has been discussed elsewhere [14], and is similar to that of the pioneering work of Drexhage [3]. Therefore, for brevity, only an outline of the techniques used to make the microcavity structures will be described. The mirror was deposited onto a silica substrate by thermal evaporation under vacuum (10^{-7} Torr) using silver (99.99% pure). The upper and lower dielectric spacer layers were deposited from 22-tricosenoic acid by the Langmuir-Blodgett (LB) technique [18]. The 22-tricosenoic acid, in a chloroform solution (concentration 0.2 mg ml^{-1}) was introduced onto a pure water subphase (18 MΩ resistivity, 18 °C, pH 5.5). The Langmuir film was compressed to a surface pressure of 30 mN m^{-1} before being transferred to the silver mirror. The film transfer was performed at a rate of

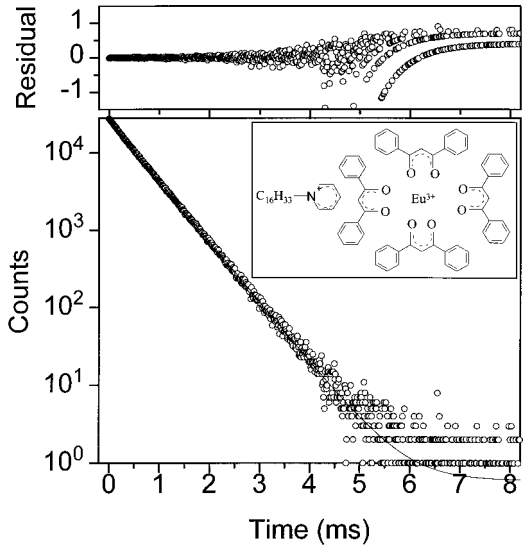

FIG. 3. The main part of the figure shows the time resolved evolution of the emission intensity from a Langmuir-Blodgett film of Eu^{3+} ions (symbols), situated in a structure similar to that shown in the inset of Fig. 1. The Eu^{3+} ion separations from the silver mirror and the air interface were 104 and 78 nm, respectively. The line displayed is a best fit of a biexponential decay to the data. The upper plot shows the residual between the theory and data. The inset shows a schematic of the Eu^{3+} chelate molecule.

0.5 mm s^{-1} onto the vertically oriented sample.

Europium ions (Eu^{3+}) were chosen as the emissive species due to their near monochromatic emission (614 nm), the predominant electric dipole nature of this transition, and relatively long fluorescence lifetime (~1 ms). The Eu^{3+} ions were incorporated within a chelate molecule, *N*-hexadecyl pyrdinium tetrakis (1,3-diphenyl-1,3-propandione) europium. The inset of Fig. 3 shows a schematic of this molecule. This molecule allowed a suitable optical pumping mechanism to be employed and also allowed the Eu^{3+} ions to be deposited by the LB technique thus allowing them to be precisely located within the microcavity structure. The chelate molecule was introduced onto the water subphase in solution (4:1 mixture of benzene and acetone). The film was compressed to a surface pressure of 10 mN m^{-1} before being transferred to the sample by a horizontal lift-off technique. Overlayers of 22-tricosenoic acid were subsequently deposited on top of the Eu^{3+} chelate layer, using the verticle deposition outlined above. This method ensured only a single monolayer of Eu^{3+} was deposited, retaining the nanometer resolution of the LB technique.

Time resolved luminescence measurements of the Eu^{3+} fluorescence were obtained using standard photon counting techniques. The sample was photoexcited using 5 ns pulses of UV light (337 nm) from a nitrogen laser. The fluorescence was collected via a lens and spectrally isolated by passing it through a spectrometer, set to pass the Eu^{3+} emission wavelength. The collected light was then focused onto a photomultiplier (Hamamatsu R955), the output from which was monitored by a standard multichannel photon counter (Stanford SR430) under computer control.

Figure 3 shows typical data for the time evolution of the intensity of Eu^{3+} emission from a LB film. Here the Eu^{3+} chelate-silver separation was 104 nm, the Eu^{3+} chelate-air separation was 78 nm. For a population of ions with identical chemical and physical environments the fluorescence should have a single exponential time dependence and indeed the data appear to the eye to agree with a single exponential decay. However, careful analysis has shown a biexponential time dependence gives a better fit to the data. A biexponential decay has the following form:

$$I(t)=y_0+A_1e^{-t/\tau_1}+A_2e^{-t/\tau_2},$$

where $I(t)$ is the intensity detected, τ_1, τ_2 are the long and short lifetime components, respectively, and A_1 and A_2 are the relative strengths of the two components. The background count is represented by y_0. The deviation from a single exponential is possibly due to contamination of a second chelate species, an unwanted by-product of the chelate manufacture, or perhaps due to ion-ion interactions. Table I shows the parameters obtained for the data presented in Fig. 3, and is fit using biexponential and single exponential functional forms. The table also contains the standard χ^2 value of the fits. By comparing the τ_1 components of the biexponential and single exponential fits we note that there is only a small difference between the two. In fitting the biexponential decay an increase in τ_1 is found when compared to the single exponential fit. This increase is typically less than 5%, a small shift compared to the large changes observed in the data of Fig. 1. We have fitted a biexponential decay to all our decay data and the lifetime we quote refers to the longer lifetime component, τ_1.

TABLE I. The parameters and their uncertainty obtained when fitting the measured time resolved decay in Fig. 3 to a single and biexponential form.

	Double exponential		Single exponential	
	Value	Uncertainty	Value	Uncertainty
y_0	0.600	0.05	0.698	0.049
A_1	24 960	290	26 950	30
τ_1 (ms)	0.5609	0.0017	0.5461	0.000 47
A_2	2800	270		
τ_2 (ms)	0.2617	0.0200		
χ^2	0.741		1.084	

V. RESULTS

A. The role of the second interface

To highlight the significance of the role played by the dielectric-air interface we have measured the SpE lifetime of the Eu^{3+} ions as a function of the distance between them and the silver surface, d_{bot}, for several different overlayer thicknesses, d_{top}. If the dielectric-air interface were of no consequence we would expect these data to be the same; however, they are markedly different, see Fig. 4. Modeling of the lifetime using the CPS theory is also displayed in Fig. 4 as full lines accompanying the experimental data points. We note the excellent agreement between experiment and theory in the regime $d_{bot}<130$ nm. The data shown in Fig. 4 were obtained from a single experimental sample, the different values of d_{top} being achieved by the subsequent addition of

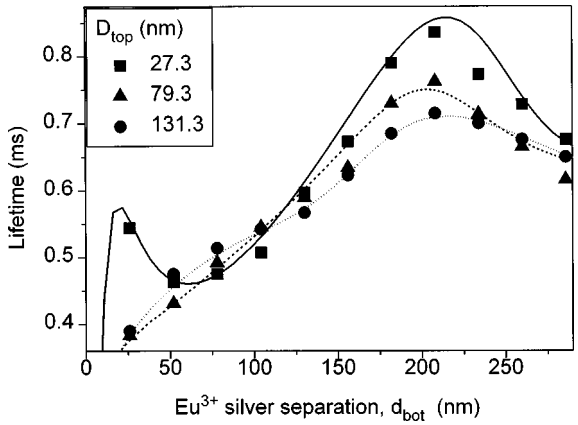

FIG. 4. The measured SpE lifetime as a function of the Eu^{3+}-ion–mirror separation for three different overlayer thicknesses, $d_{top}=26$, 79, and 130 nm. Experimental data points are represented by the symbols and the lines are the associated results from the CPS model. The figure shows the importance of the dielectric-air interface.

extra overlayers. This ensures that changes in the measured decay rate are the result of different optical environments caused by the location of the dielectric-air interface.

By comparing the data for the three values of d_{top} shown in Fig. 4 we observe a flattening of the first peak that occurs at $d_{bot}=20$ nm, as overlayers are added. At these small Eu^{3+}-silver separations, coupling to the SPP mode dominates other coupling mechanisms [11], see Fig. 2(b). We can attribute the flattening of the first peak with the increase in strength of the electric fields associated with the SPP mode as the overlayer becomes thicker [11]. Figure 4 also shows a general reduction in the SpE lifetime as the overlayer thickness is increased. This reduction is caused by an increase in the effective refractive index sampled by the electric field of the dipole.

B. Fixed dielectric thickness

As mentioned above, the dispersion of the EM modes is independent of the location of the emitter within a given structure. The SpE decay rate for a dipole embedded within the dielectric of such a system is then only dependent on the coupling strength between it and the different EM modes [15]. Figures 5(a) and 5(b) show the measured SpE decay rate for a range of emitter locations (d_{bot}) in two fixed thickness structures, $d_{total}=104$ and 156 nm, respectively. The lines accompanying the data points show the modification to the SpE rate calculated with the CPS model.

As previously described, the CPS model can be used to calculate the contribution to the SpE rate, $I(u)$, as a function of u. To calculate the SpE rate $I(u)$ is integrated over all positive values of u. In doing so, all information concerning the modal contribution is lost. To retain information concerning the coupling of the emitter to the different EM modes of the system we have integrated $I(u)$ over selected ranges of u, corresponding to the different modes. Figures 5(a) and 5(b) also display the contribution to the decay rate of the radiative, waveguide, and SPP modes calculated this way. In addition there is a contribution to the SpE decay rate that does not arise from coupling to EM modes [11]. This contribution

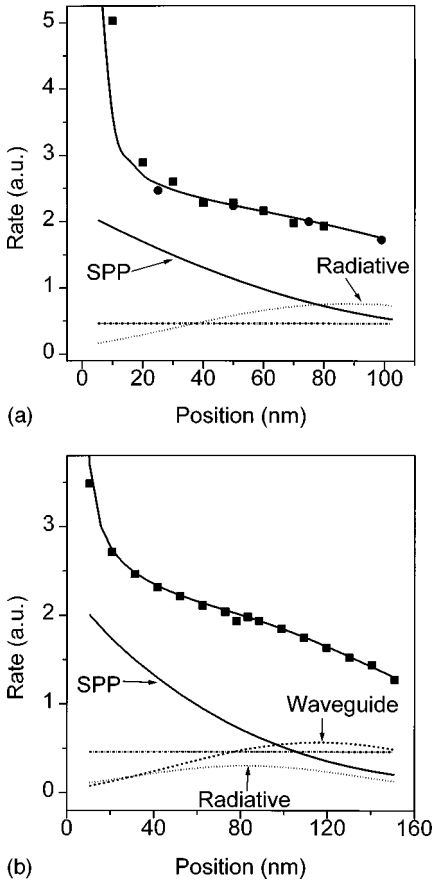

FIG. 5. The measured SpE decay rate of Eu^{3+} ions embedded within a sample having a constant dielectric thickness, (a) $d_{total}=104$ nm and (b) $d_{total}=156$ nm. The x axis displays the position of the ions within the dielectric with respect to the metal interface. The symbols are the experimental data points and the lines show both the contributions to the decay rate of the modes and the total decay rate, evaluated by the CPS theory. The solid, dashed, dotted, and dash-dotted lines represent the SPP, first waveguide, radiative, and the intrinsic nonradiative contributions, respectively. Note the 104-nm thickness, (a), is too thin to support a waveguide mode.

is given by the term $(1-q)$, as shown in Eq. (1). It is independent of the optical mode density and is a constant for all the results presented in this paper and is shown by a dash-dotted line in Fig. 5. For Eu^{3+}-silver separations of less than 20 nm coupling to lossy surface waves begins to contribute to the SpE rate. These lossy surface waves occur at very high values of u, typically $u>20$ [11]. The coupling to these lossy surface waves accounts for the discrepancy between the SpE rate (integrated over all values of u) and the sum of the modal contributions which occurs for small Eu^{3+}-mirror separation. Note that the sample having a dielectric total thickness $d_{total}=104$ nm is too thin to support any waveguide modes, therefore the SpE rate is simply the sum of the SPP and the radiative contributions. In contrast, the greater thickness of the 156-nm-thick sample enables it to support one guided mode, see Fig. 2(b), which contributes significantly to the SpE rate. As expected, the contribution of the SPP in both cases dominates for $d_{bot}<100$ nm, leading to a much increased decay rate (shorter lifetime). In Fig. 5(b), for $d_{bot}<100$ nm, although there is a large contribution from the SPP mode, the radiative and guided modes also make sig-

nificant contributions to the SpE rate. The selective integration technique we have used here has been used before [11]; the results shown in Figs. 5(a) and 5(b) show the power of this technique in assessing the contribution of the different EM modes to the measured decay rate.

We also note that in Fig. 5(a) there are two sets of symbols (squares and circles) that correspond to data obtained from two different sets of experimental samples. Comparison of the two data sets shows that we have obtained good consistency from sample to sample for our microcavity structures. In general we have found sample to sample consistency to be limited by the variation in optical parameters of the silver films fabricated during different depositions.

C. Introduction of waveguide modes

For high Q microcavities the introduction of waveguide modes as the cavity thickness increases leads to significant sharp features in the spontaneous emission decay rate, Fig. 2(a). The data displayed in Fig. 1 have none of the sharp features [see also Fig. 2(b)] that have been observed for high Q cavities [7]. In Sec. IV A we saw that for a thickness (d_{total}) of 156 nm there is significant coupling to all of the EM modes even if the Eu^{3+} ions are located near the dielectric-air interface. We can therefore conclude that the absence of these sharp features is not a consequence of fixing the location of the Eu^{3+} ions at the dielectric-air interface, the situation that applies for the data of Fig. 1. To further investigate the lack of sharp features we have measured the decay rate for emitters embedded within our asymmetric microcavity system for different total thicknesses (d_{total}) of the dielectric layer, spanning the transition from a nonguiding structure to a guiding one.

We concentrated our study on dielectric layers in the range associated with the introduction of the first two guided modes. Figures 6(a) and 6(b) show the measured SpE rate for structures in which d_{top} is increased and d_{bot} is fixed at 104 and 130 nm, respectively. The experimental data are presented together with the accompanying CPS theory. The data sets are plotted as a function of the total dielectric thickness (d_{total}). This has been chosen in preference to d_{bot} as we are concerned with the introduction of the guided modes whose dispersion depends on the value of d_{total}. Also displayed in the figures is the calculated contribution of the different EM modes. Here for clarity the contribution to the decay rate by the intrinsic nonradiative term has been omitted. Note the introduction of the guided modes at thicknesses of approximately 110 and 220 nm. Figures 6(a) and 6(b) clearly show that as coupling to the guided modes becomes important there is an associated reduction in coupling to the radiative modes. This tradeoff between the different types of mode accounts for the fact that there is no significant modification in the SpE rate as a function of d_{total}, for this microcavity structure.

VI. DISCUSSION

We have obtained an extensive set of experimental data of the SpE rate for a range of samples, and for each we have obtained a good match between the CPS theory and our data. This allows us to be confident in our use of the CPS theory to assess the contribution of all the EM modes on the SpE rate

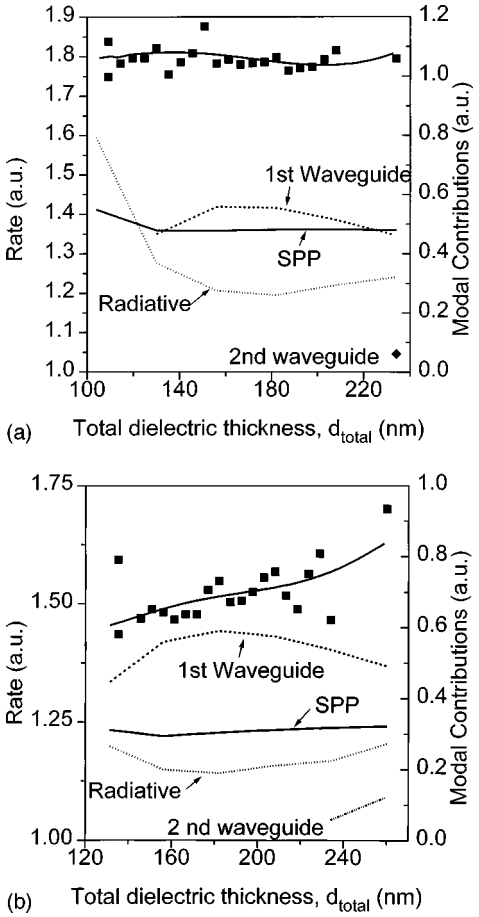

FIG. 6. The measured SpE decay rate as a function of the total dielectric thickness for Eu^{3+} ions located at a fixed distance from the metal, (a) $d_{\text{bot}}=104$ nm and (b) $d_{\text{bot}}=130$ nm. The points represent the experimental data and the line accompanying them displays the rate calculated using the CPS theory, plotted using the left- hand axis. The modal contributions are plotted using the right-hand axis with solid, dashed, dotted, and dash-dotted lines representing the SPP, first waveguide, radiative, and the second waveguide mode, respectively. The contribution of the second waveguide is shown as a diamond point for clarity in (a), as it is only close to the maximum total thickness (230 nm) that this mode exists.

of the embedded emitters using the selective integration technique outlined above. Our results have demonstrated that the SpE rate of an emitter is sensitive to relatively small changes in its local optical environment as the latter controls the EM modes available to the emitter. An emitter embedded within a thin dielectric layer above a metal mirror may lose its energy to the following EM modes: (1) Radiative (including leaky) modes, (2) bound waveguide modes, and (3) the SPP mode. The data presented above have been obtained from structures spanning a large range of dielectric thicknesses (d_{total}) with the emissive layer located at various positions within the microcavity. Over this range of microcavity structures, the EM mode that provides the dominant decay channel for the SpE rate changes. For small Eu^{3+}-silver separations (d_{bot}) the SPP mode dominates, due to the surface mode nature of the SPP and the strong electric fields associated with it. This is clearly shown by the fixed dielectric thickness data (Sec. IV B). Depending on the

thickness of the sample, either radiative or waveguide modes may dominate for larger values of the Eu^{3+}-silver separations, a point we shall return to below.

The modal contribution to the SpE decay rate thus depends on two factors, first, the sample geometry which controls the dispersion of the EM modes of the microcavity system, and second, the coupling of the emitter to the modes is dependent on the magnitude of the electric field of the mode at the location of the emitter. This in turn is controlled by the position of the emitter within the microcavity. We investigated these two factors by taking advantage of the nanometer resolution in both the cavity thickness and the location of the emissive layer that our fabrication technique afforded.

We have also shown that the selective integration technique can be used to determine the probability that an emitter will lose its energy to a specific decay channel. The importance of this technique arises from the difficulty of directly measuring the power coupled to the nonradiative EM modes. The major difficulty is that although the spatial distribution of the emitted radiation (radiative modes) can be measured directly, a mechanism to couple guided modes to radiative ones must be provided before the former can be measured. Two common coupling mechanisms are grating [19] and prism coupling [20]. Measuring the power coupled out in this way may not give an accurate measure of the modal contribution to the SpE decay. Such inaccuracies may be caused by a combination of incomplete coupling and the presence of intrinsic absorption which will act to dissipate the modes before significant coupling occurs. A further difficulty with intensity based studies occurs if photoexcitation is used because enhancement and inhibition of the absorption of the pump radiation by the emitter due to the microcavity [20] complicate the comparison of different microcavity structures. These difficulties are not present when measuring the SpE rate, since it is not dependent on any of these secondary processes. Thus, although an indirect measure of the modal contribution, the selective integration technique can be a powerful tool in the design of emissive microcavity devices.

As an example we can reexamine one structure reported in Sec. V C. We choose the sample with $d_{\text{total}} = 234$ nm, a thickness that allows the structure to support two waveguide modes. Further, the emissive layer is located such that $d_{\text{bot}} = 104$ nm. Using selective integration we find the contributions to the SpE rate are

Radiative modes	18%
2nd waveguide mode	3%
1st waveguide mode	26%
SPP mode	27%
Intrinsic nonradiative $(1-q)$	26%

As a consequence of the difficulties discussed above, only a limited number of studies have directly measured the emission into the different EM modes of a microcavity. In one example of such measurements Rigneault *et al.* [20] studied a planar dielectric microcavity. They reported that up to 33 times more power is emitted into the guided modes supported by the structure than is emitted as radiation. This is considerably different from our results, e.g., those listed above, where only three times more power is coupled to the bound modes of the microcavity than is emitted as radiation. The difference in these ratios is due to the different structures examined. The relatively high fraction of power radiated from our structures is due primarily to the reduced number of guided mode supported by our thinner microcavity.

Sullivan and Hall [21] have also used a selective integration technique in their study of a fluorescence biosensing scheme. They examined the emission from a laser dye separated from a silver mirror by a thin layer of LiF. They found a significant enhancement in the emitted intensity (up to a factor of 450) when compared to a sample without a silver mirror. The enhancement could only be accounted for by assuming the power lost by the laser dye to the bound modes of the system underwent secondary coupling. This occurred as a result of the bound EM modes scattering off the intrinsic roughness of the LiF to produce radiation. In devices such as the microcavity light-emitting diode (LED) the photoluminescence yield may be limited by coupling to bound EM modes [22]. As we have demonstrated, the selective integration technique can be used to assess the extent of this coupling. It can thus be used to estimate by how much the photoluminescence yield could be enhanced if the bound modes were to be coupled to radiation, for example, through grating coupling.

VII. SUMMARY

Experimental results for the SpE rate of Eu^{3+} ions embedded within a dielectric planar layer above a silver mirror have been presented, both as a function of the thickness of the dielectric layer and the location of the ions embedded within it. We have demonstrated that the presence of the dielectric-air interface has a significant effect on the spontaneous decay rate of the Eu^{3+} ions. Further, we have recognized that the silver-dielectric-air structure is in fact an asymmetrical microcavity. By finding good agreement between our SpE rate data and predictions based on a well-established classical theory, we have been able to calculate the contribution of the various decay channels to the overall decay rate.

We focused our attention on the role that waveguide modes play in the decay process. As the thickness of the dielectric layer is increased the modes change in character from radiative to fully guided. We have shown that as this transition takes place there is no corresponding abrupt change in the SpE rate, as has been seen for the more commonly studied symmetric microcavity. Rather, as the transition takes place, there is a redistribution of the fraction of power dissipated between the radiative and guided modes.

ACKNOWLEDGMENTS

We wish to thank the EPSRC and the University of Exeter for financial support. We are also very grateful to Piers Andrew for helpful discussions.

[1] E. M. Purcell, Phys. Rev. **69**, 681 (1946).
[2] E. Fermi, Rev. Mod. Phys. **4**, 87 (1932).
[3] K. H. Drexhage, in *Progress in Optics XII*, edited by E. Wolf (North-Holland, Amsterdam, 1974), p. 165.
[4] R. R. Chance, A. Prock, and R. Silbey, Adv. Chem. Phys. **37**, 1 (1978).
[5] K. H. Drexhage, M. Fleck, H. Kuhn, F. P. Schäfer, and W. Sperling, Ber. Bunsenges. Phys. Chem. **20**, 1179 (1966); K. H. Drexhage, H. Kuhn, and F. P. Schäfer, *ibid.* **72**, 329 (1968).
[6] A. P. Alivasatos, M. F. Arndt, S. Efrima, D. H. Waldeck, and C. B. Harris, J. Chem. Phys. **86**, 6540 (1987).
[7] E. A. Hinds, Adv. At., Mol., Opt. Phys. **28**, 237 (1991).
[8] F. B. Seeley, J. E. Alexander, R. W. Connaster, J. S. Conway, and J. P. Dowling, Am. J. Phys. **61**, 545 (1993).
[9] S. M. Dutra and P. L. Knight, Phys. Rev. A **53**, 3587 (1996).
[10] H. Becker, S. E. Burns, and R. H. Friend, Phys. Rev. B **56**, 1893 (1997).
[11] G. W. Ford and W. H. Weber, Phys. Rep. **113**, 197 (1984).
[12] E. D. Palik, *Handbook of Optical Constants of Solids* (Academic, London, 1991).
[13] W. L. Barnes and J. R. Sambles, Surf. Sci. **177**, 399 (1986).
[14] R. M. Amos and W. L. Barnes, Phys. Rev. B **55**, 7249 (1997).
[15] M. S. Lidzey, D. D. C. Bradley, M. A. Pate, J. P. R. David, D. M. Whittaker, T. A. Fisher, and M. S. Skolnick, Appl. Phys. Lett. **71**, 744 (1997).
[16] K. R. Welford and J. R. Sambles, J. Mod. Opt. **35**, 1467 (1988); also S. C. Kitson, W. L. Barnes, and J. R. Sambles, J. Appl. Phys. (to be published).
[17] H. Raether, *Surface Plasmons* (Springer-Verlag, Berlin, 1988).
[18] K. Blodgett and I. Langmuir, Phys. Rev. **51**, 964 (1937).
[19] A. Adams, J. Moreland, P. K. Hansma, and Z. Schlesinger, Phys. Rev. B **25**, 3457 (1982).
[20] H. Rigneault, S. Robert, C. Begon, B. Jacquier, and P. Moretti, Phys. Rev. A **55**, 1497 (1997).
[21] K. G. Sullivan and D. G. Hall, J. Opt. Soc. Am. B **14**, 1160 (1997).
[22] A. Dodabalapur, Solid State Commun. **102**, 259 (1997).